

Water Resources Research®

RESEARCH ARTICLE

10.1029/2023WR036214

Where in the World Are Vegetation Patterns Controlled by Hillslope Water Dynamics?



Key Points:

- A catchment-based strategy is proposed to represent explicit land cover heterogeneity using discretized height bands along a hillslope
- Landscapes shaped by hillslope water dynamics are detected in many regions of the world in diverse climate zones
- The proposed strategy can concisely resolve land cover heterogeneity in land surface modeling with relatively high accuracy

Supporting Information:

Supporting Information may be found in the online version of this article.





Correspondence to:

S. Li,
shuping@rainbow.iis.u-tokyo.ac.jp

Citation:

Li, S., Yamazaki, D., Zhou, X., & Zhao, G. (2024). Where in the world are vegetation patterns controlled by hillslope water dynamics? *Water Resources Research*, 60, e2023WR036214. <https://doi.org/10.1029/2023WR036214>

Received 8 SEP 2023
Accepted 15 MAR 2024

Shuping Li¹ , Dai Yamazaki² , Xudong Zhou² , and Gang Zhao² 

¹Department of Civil Engineering, The University of Tokyo, Tokyo, Japan, ²Institute of Industrial Science, The University of Tokyo, Tokyo, Japan

Abstract Some recent land surface models can explicitly represent land surface process and focus more on sub-grid terrestrial features. Many studies have involved the analysis of how hillslope water dynamics determine vegetation patterns and shape ecologically and hydrologically important landscapes, such as desert riparian and waterlogged areas. However, the global locations and abundance of hillslope-dominated landscapes remain unclear. To address this knowledge gap, we propose a globally applicable method that employs high-resolution elevation, hydrography, and land cover data to concisely resolve explicit land cover heterogeneity for the mapping of hillslope-dominated landscapes. First, we aggregate pixels into unit catchments to represent topography-based hydrological units, and then vertically discretize them into height bands to approximate the hillslope profile. The dominant land cover type in each height band is determined, and the uphill land cover transition is analyzed to identify hillslope-dominated landscapes. The results indicate that hillslope-dominated landscapes are distributed extensively worldwide in diverse climate zones. Notably, some landscapes, including gallery forests in northeastern Russia and desert riparian in the Horn of Africa, are newly revealed. Furthermore, the proposed strategy enables more accurate representation of explicit land cover heterogeneity than does the simple downscaling of a rectangular grid from larger to smaller units, revealing its capability to concisely resolve land cover heterogeneity in land surface modeling with relatively high accuracy. Overall, we present the extensive global distribution of landscapes shaped by hillslope water dynamics, underscoring the importance of the explicit resolution of heterogeneity in land surface modeling.

Plain Language Summary Local land cover distributions are influenced profoundly by various factors that are not represented fully in current land surface models. In alpine regions, changes in vegetation layers from mountain bases to tops are apparent; this phenomenon is driven largely by climatic factors, such as temperature. Interestingly, similar vegetation changes occur in relatively flat regions due to uneven water distribution on hillslopes. Hillslope water dynamics contribute to the development of unique landscapes, such as gallery forests, and substantially influence local ecological and hydrological conditions. Despite this importance, the global locations and abundance of such landscapes remain mysterious. In this study, we propose a method for the mapping of the global distribution of hillslope-dominated landscapes using high-resolution land-cover, terrain, and climate data. The results reveal that the global distribution of these landscapes, including some newly revealed landscapes such as gallery forests in northeastern Russia, is extensive. In conclusion, our study sheds light on the significant role of hillslope water dynamics in determining vegetation patterns in many parts of the world, highlighting the importance of resolving local features in land surface modeling.

1. Introduction

Land surface models (LSMs) are integrated with climate models as the land components for the simulation of land–atmosphere water and energy exchange. For global- or continental-scale modeling, these models generally operate on large (~25–200-km) grid units (Bacmeister et al., 2018; Kay et al., 2015). However, LSMs have a limited ability to capture fundamental land surface processes that are heterogeneous, such as hydrological processes, which are linked closely to spatially complex factors such as topography, land cover, and soil properties. These processes occur at sub-grid scales and are not readily resolved using current models (Clark et al., 2015; Fan et al., 2019; Fisher & Koven, 2020; Wood et al., 2011).

At the sub-grid scale, land surface heterogeneity is profoundly differentiated by factors such as local climatic, topographic, and hydrological conditions (Fisher & Koven, 2020; Gao et al., 2014; Li & Sawada, 2022; Tai

© 2024. The Authors.

This is an open access article under the terms of the [Creative Commons Attribution-NonCommercial-NoDerivs License](https://creativecommons.org/licenses/by/4.0/), which permits use and distribution in any medium, provided the original work is properly cited, the use is non-commercial and no modifications or adaptations are made.

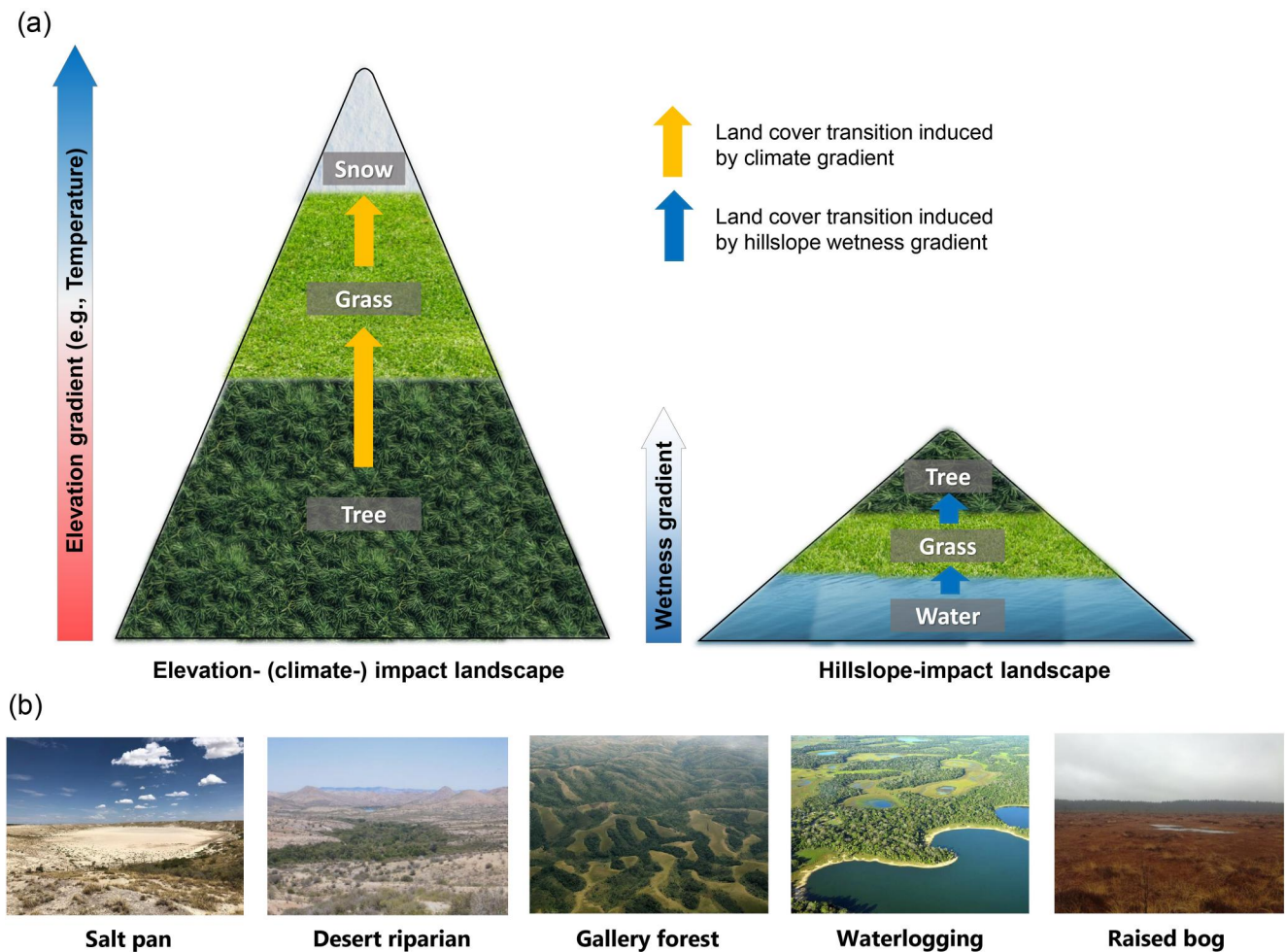


Figure 1. (a) Examples of landscapes dominated by elevation (climate) and hillslope dynamics. Temperature is considered to be the factor controlling uphill land cover transition in climate-dominated landscapes, and wetness is regarded as the major controller of hillslope-dominated landscapes. Note that we selected one pathway of land cover transition for illustration; many other paths for elevation- and hillslope-dominated landscapes exist. (b) Typical landscapes shaped by hillslope water dynamics: salt pan (SP; salt lakes of Pinos Wells; photograph by David Ryan, <https://gentleartofwandering.com/wandering-around-the-salt-lakes-of-pinos-wells/>, used with permission), desert riparian (DR; forest corridor in arid Arizona, https://en.wikipedia.org/wiki/Desert_riparian), gallery forest (GF; forest corridor in the Luama Katanga Reserve of eastern Congo; photograph by Andrew Plumtre/WCS, <https://news.mongabay.com/2014/11/mapping-mistake-leaves-wildlife-at-risk/>, used with permission), waterlogging (WL; oxygen-stressed environment in Pantanal, <http://wikimapia.org/8582923/Pantanal-Mato-Grossense-National-Park>), and raised bog (RB; uplifted peatland in Teijo National Park, Finland, https://en.wikipedia.org/wiki/Raised_bog). We use the same images of DR, GF, and WL in Figure 2 by Fan et al. (2019), because they are considered as the most appropriate examples to illustrate the corresponding hillslope-dominated landscapes. The images represent climatic gradients from hot and dry on the left to cold and wet on the right.

et al., 2020). In mountainous regions with significant topographic relief, climatic gradients tend to determine vertical vegetation zonation from the valley to hilltop (see Figure 1a, von Humboldt, 1807; Schimper et al., 1903; Zou et al., 2023). In regions where the terrain is much flatter, which are governed by hillslope-scale water dynamics, such vegetation gradients are also observed at the sub-grid scale (see Figures 1a and Fan et al., 2017), as gravity drives vertical and lateral surface and subsurface water flow downhill, leading to a wetter (and sometimes more saline) valley and drier hill.

In light of the importance of addressing the fundamental phenomenon underlying these patterns at the sub-grid scale, model developers have recently aimed to resolve the high-resolution land surface heterogeneity in LSMs (Ajami et al., 2016; Burton et al., 2019; Chaney et al., 2016; Hazenberg et al., 2015; Lawrence et al., 2019; Naudts et al., 2015; Subin et al., 2014; Swenson et al., 2019). In particular, the concept of a representative hillslope, commonly incorporated into hydrological models, has been applied to LSMs. This concept is used to aggregate

hydrologically similar areas in single catchments into hydrological response units, allowing the catchment area draining into the main channel to be treated as an integral hillslope. This representation consists of multiple vertical bands with varying widths and elevations, and water is routed linearly from higher to lower bands. By treating the band as the basic modeling unit for the incorporation of representative hillslopes into LSMs, this method can efficiently resolve the explicit land surface heterogeneity and the key hydrological processes occurring at the hillslope scale (Newman et al., 2014). This method has been applied in some studies, resulting in considerable reduction of the computational cost of the LSM (Hazenberg et al., 2015; Swenson et al., 2019). Furthermore, Chaney et al. (2018) divided the hillslope into connected bands and then aggregated the hyper-resolution pixels with similar hydrological behavior in each band into complex tiles or clusters for the more efficient representation of land surface processes. This method improves computational efficiency while minimizing the degradation caused by simulation at high resolution, providing promising results for the resolution of heterogeneous land-surface processes at local and regional scales. Nevertheless, previous hillslope modeling studies have focused on model development, and relevant analysis of the global distribution of hillslope-dominated landscapes remains lacking. Research aiming to close the gap between model simulation results and the impacts on sub-grid land cover heterogeneity would provide great benefit.

Plant growth is strongly suppressed under extremely dry (plant water stress), humid (plant water excess), and saline conditions, leading to the development of unique landscapes (Figure 1b; detailed information is provided in Supplementary Text S1 in Supporting Information S1). For example, under arid or semiarid climate conditions, drier uphill areas constrain plant growth, forming desert riparian (DR) and gallery forest (GF) landscapes. When excess water accumulates in down-valley or upper hill areas, plants drown due to limited root respiration, leading to the development of waterlogging (WL) or raised bog (RB) landscapes, respectively. Salt pan (SP) landscapes develop due to excessive evaporation relative to groundwater inflow and precipitation, which causes saline soil conditions in down-valley areas and hinders plant growth. Given their key roles in influencing local land-atmosphere water and energy budgets and global biogeochemical cycles (Clark et al., 2015; Gao et al., 2018), these landscapes have been studied separately and regionally, with examination of their spatiotemporal distribution and evolution using state-of-the-art remote sensing techniques (Kirpotin et al., 2021; Lehner & Döll, 2004; Macfarlane et al., 2017; Nguyen et al., 2015; Safaee & Wang, 2020; Xu et al., 2018). As noted by Fan et al. (2019), such landscapes (Figure 1b) are likely to exist in diverse parts of the world. However, their distribution patterns and abundance have not been assessed to date. We still lack a global overview of hillslope-dominated landscapes, which is necessary to fully elucidate how hillslope water dynamics affect land surface heterogeneity.

In this study, the global tessellation of catchments and height bands are generated based on up-to-date high-resolution topographic data from the MERIT DEM and hydrographic data from MERIT Hydro (Yamazaki et al., 2017, 2019). Using those data combined with high-resolution land cover and climate classification maps, we aim to construct a global distribution map of hillslope-dominated landscapes and discuss the importance of explicitly resolving land surface heterogeneity in land surface modeling. First, we propose an aggregation method called the catchment-based strategy, which is used to derive a global distribution map of landscapes shaped by hillslope water dynamics. Second, to assess and verify the detection results, we calculate the detection accuracy with the aid of visual examination. Third, to determine the abundance of hillslope-dominated landscapes, we construct a global distribution map of landscapes shaped by climate impacts for comparison. Finally, through comparison of the catchment-based strategy (downscaling of catchment to 10 height bands) with the simple downscaling of an equivalent size of rectangular grid to 9 sub-grids, we try to demonstrate the superiority of applying height bands to resolve the land cover heterogeneity.

2. Data

The datasets used in this study are listed in Table 1.

We employed the MERIT DEM dataset as our topographic data. Major error components of other DEMs have been eliminated from this dataset through the separation of types of bias (absolute and tree height) and noise (stripe and speckle) using multiple satellite datasets and filtering techniques (Yamazaki et al., 2017). In particular, significant improvements have been achieved in flat regions with height errors exceeding their topographic variability, and landscapes such as river networks and hill-valley structures are represented clearly.

Table 1
Data Sets Used in This Study

Data set	Name	Spatial resolution	Temporal range	Reference
Topography	MERIT DEM	3 arcsec	–	Yamazaki et al. (2017)
Hydrography	MERIT Hydro	3 arcsec	–	Yamazaki et al. (2019)
Land cover	LULC Sentinel-2	10 m	2017–2022	Karra et al. (2021)
Climate classification	Koppen–Geiger map	1 km	1980–2016	Beck et al. (2018)
Optical satellite image	Google static map	–	–	–

We used MERIT Hydro as our hydrographic data, representing the global hydrographic network. These data are derived from the MERIT DEM and water body datasets (G1WBM, Global Surface Water Occurrence, and OpenStreetMap). Due to the increasing availability of high-quality baseline geospatial datasets, this dataset has more spatial coverage (between 90°N and 60°S) and representation of small streams than do other datasets (Yamazaki et al., 2019).

The land use/land cover (LULC) product derived from ESA Sentinel-2 imagery was used as the land cover data (Karra et al., 2021). A global LULC map was created based on a large novel dataset of more than 5 billion human-labeled Sentinel-2 pixels, with a high resolution of 10 m. The LULC data represents 11 types of land cover: clouds, snow/ice, bare ground, built areas, scrub/shrub areas, crops, flooded vegetation, grass, trees, water, and oceans. LULC products from 2017 to 2022 are available; we used the 2020 product in our analysis. To consistently match the spatial resolution of the MERIT DEM and MERIT Hydro data, the LULC data were aggregated from 10 m to 3 arcsec (i.e., 90 m at the equator) using the nearest-neighbor interpolation method.

To account for climate impacts, we used the present-day Koppen–Geiger map as described by Beck et al. (2018). The map was generated from an ensemble of four high-resolution, topographically corrected climatic maps, and has greater classification accuracy and more detailed information than do previous versions, especially in regions with sharp spatial or elevation gradients. To maintain consistency with the MERIT DEM and MERIT Hydro data, this map was resampled from 1-km to 3-arcsec spatial resolution.

In general, the topographic, hydrographic, land cover and climate classification data are used for landscape detection, as described in Section 3. In Section 4, the results obtained with the combined application of satellite imagery, topographic and land cover information are evaluated and discussed.

3. Methods

3.1. Catchment-Based Strategy

Land surface processes are commonly modeled in LSMs based on a large rectangular grid, with the topographic factor parameterized uniformly within each grid cell (Takata et al., 2003; Wood et al., 2011). In this case, the major river channel in each grid unit is not determined explicitly, and relative height above the river channel cannot be defined. Without explicit consideration of the main river channel and hillslope drainage into the channel in each calculation unit, an LSM cannot resolve observed land cover heterogeneity that is shaped by hillslope water dynamics. Thus, in this study, we propose a catchment-based strategy for LSMs that can concisely resolve the sub-grid heterogeneity related to hillslope water dynamics, as follows.

- 1) Based on the MERIT Hydro high-resolution hydrographic dataset, the flow directions of pixels are merged to create a terrestrial boundary map of unit catchments using the flexible location of waterways (FLOW, Yamazaki et al., 2009) upscaling method. By maintaining uniform catchment size and river channel connectivity, FLOW allocates outlets throughout river networks to define the main river channels of unit catchments. As a result, each rectangular grid unit is spatially paired with one unit catchment of similar size (Figure 2a). Although the catchment boundary map can be created flexibly to discretize unit catchments into multiple sizes, in this study we discretize unit catchments to match the 0.25° rectangular grid units. One reason is that the size of 0.25° is the lower end of the widely used spatial range in some earth system models such as CESM (Bacmeister et al., 2018; Kay et al., 2015). Within this size of grid, previous studies had addressed the

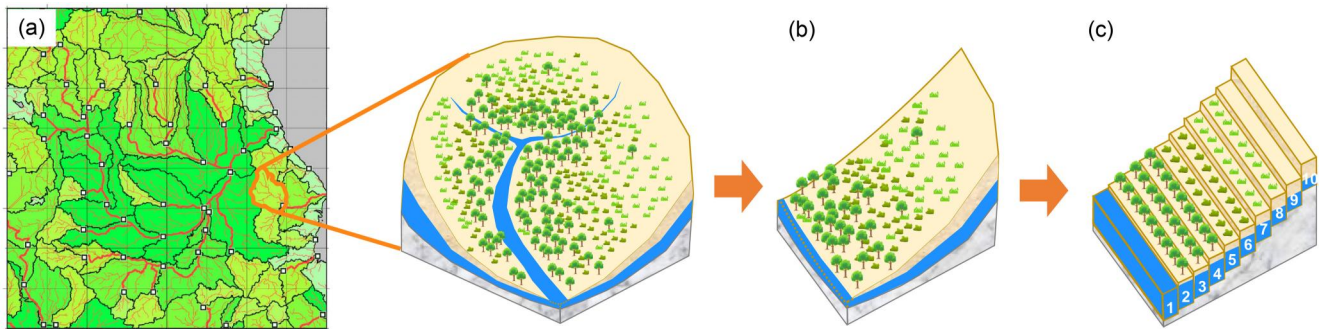


Figure 2. Schematic diagram of the catchment-based strategy. (a) The terrestrial area is first segmented into unit catchments of similar sizes; (b) the representative hillslope is applied as a conceptual approximation of the unit catchment; and (c) the representative hillslope is discretized vertically into 10 height bands, each with uniform surface area.

sub-grid heterogeneity (Chaney et al., 2018). Setting the unit size to 0.25° might be appropriate to bridge the earth system modeling and the resolution of sub-grid heterogeneity.

- 2) A catchment generally consists of numerous complex hillslope forms, among which land cover transitions from channel to ridgeline are assumed to be highly similar. For conceptual clarity and computational efficiency, these complex hillslope forms are theoretically collapsed into a concise representative hillslope based on the relative height above the main river channel (Figure 2b).
- 3) The representative hillslope is discretized into 10 vertical height bands. Because hillslope water converges at the nearest stream point rather than the lowest point of the catchment, soil wetness generally aligns with the distance to the nearest stream point. Thus, for height band discretization we use relative elevation to nearest stream point rather than actual elevation. To evenly discretize height bands, we fix the area in each height band to uniform value (Figure 2c).
- 4) The proportion of each land cover type in each band is summarized, and the dominant land cover type (that accounting for the largest proportion) is identified. To concisely and efficiently represent the explicit land cover heterogeneity using height bands, we assume that the land cover of pixels within each band is represented uniformly by the dominant land cover type (Figure 2c).

3.2. Search for Hillslope-Dominated Landscapes

For the five major hillslope-dominated landscape types (Figure 1b), information regarding the transition paths of dominant land cover types from lowland to highland was obtained from relevant studies (i.e., Fan et al., 1997, 2017, 2019; Rodríguez-González et al., 2010; MacKay, 2013; Schulz et al., 2015; Roebroek et al., 2020; Safaee & Wang, 2020; van der Velde et al., 2021) and summarized in Table 2.

Some land cover types share similar characteristics of plant adaptation to water excess or stress (e.g., in GF Path I, the grass and shrub herbaceous plant types on the upper hillslope can both withstand water stress) and should be merged as one type to represent the dominant land cover in one height band. Otherwise, in case any of the characteristically similar land cover types is individually too small in proportion to be identified as the dominant type, it might falsely skip the search and exclude some potential hillslope-dominated landscapes from the detection results. By summing the proportions of these LULC types within a height band, the characteristically similar land cover types are merged into one type prior to landscape detection.

The procedure for hillslope-dominated landscape detection is as follows.

- 1) For each unit catchment (representative hillslope), the proportion of each land cover type in each height band is calculated. The land cover type with the largest proportion is defined as the dominant land cover type.
- 2) Similar to step 1, the proportion of each climate type in each height band is calculated and the dominant type is identified.
- 3) Starting from the lowest band and stopping flexibly at any upper band, if the uphill transition of the dominant land cover type matches any path listed in Table 2, the unit catchment is maintained as a preliminarily detected hillslope-dominated landscape. Note that DR and GF share identical transition paths, but develop under different climatic conditions (Fan et al., 2019); therefore, these classes are first detected and then differentiated

Table 2
Summary of Vertical Land Cover Transition Paths for Five Hillslope-Dominated Landscape Types

Abbreviation	Salt pan SP	Desert riparian (Arid/ semiarid) DR	Gallery forest (Seasonally dry) GF	Waterlogging WL	Raised bog RB
Path I	Shrub ↑ Bare ground		Grass + Shrub ↑ Tree	Tree * ↑ Water + Flooded veg.	Flooded veg. ↑ Tree
Path II	-		Grass + Shrub ↑ Tree	Tree ↑ Grass + Shrub	Flooded veg. ↑ Grass + Shrub
Path III	-		Water + Flooded veg. ↑ -	Water + Flooded veg. ↑ -	Tree ↑ Flooded veg.
Path IV	-		-	-	Water + Flooded veg. ↑ Flooded veg. ↑ Grass + Shrub ↑ Tree ↑ Water + Flooded veg.
PTV	40%	40%	30%	30%	30%
Reference	Fan et al. (1997) Schulz et al. (2015) Safae and Wang (2020)		MacKay (2013) Fan et al. (2019) Roebroek et al. (2020)	Rodríguez-González et al. (2010) Fan et al. (2017, 2019)	van der Velde et al. (2021)

Note. Flooded veg. in the Sentinel-2 LULC data incorporates MacKay (2013) multiple flooded vegetation types, such as swamps and bogs. For WL Path I, labeled with “*”, the proportion of flooded vegetation should be larger than 0. The optimal proportion threshold value (PTV) for the detection of each landscape type is determined in the validation step and summarized here.

- based on arid/semiarid or seasonally dry climate conditions, respectively, with reference to the Köppen-Geiger climate map.
- The preliminarily detected landscapes are evaluated by setting a proportion threshold value (PTV) for the dominant land cover type in each band. Detected landscapes are invalidated and removed when the proportion of the dominant land cover type falls below the PTV. Note that this process leads to the non-detection of some landscapes if the PTV is set too high. To explore the optimal value, we tested PTVs of 20%, 30%, 40%, 50%, and 60% for the detection of each landscape type. The optimal PTV for each landscape type is discussed in Section 4.2 and summarized in Table 2.
 - The PTV is set to examine the proportion of the dominant climate type for further evaluation of the detected landscapes in step 6. Spatially, the climate type distribution is more homogeneous than the land cover distribution, and uphill transition trends are expected to be less frequent for the former than the latter (e.g., the climate type distribution is uniform for the hillslope-dominated landscape illustrated in Figure 1a). Thus, to minimize the bias caused by heterogeneity in the climate type distribution and the risk of false detection of hillslope-dominated landscapes, we set the PTV as high as 90% to define the dominant climate type in each height band.

- 6) The preliminarily detected landscapes are evaluated, and those satisfying any of the following conditions are excluded:
 - Following the uphill transition of the dominant land cover type shown in Table 2, a change in the dominant climate type occurs. This rule aims to exclude climate impacts to focus on the impact of hillslope water dynamics in the catchment. Note that the hillslope dynamics may drive a land cover transition on the lower hillslope while climate drives a land cover transition on the upper hillslope; in such cases, the unit catchments are classified as both climate-dominated and hillslope-dominated landscapes. To focus on the impact of hillslope water dynamics, such mixed catchments are treated uniformly as hillslope-dominated landscapes.
 - The integrated proportion of built area and cropland in any height band exceeds 1%. Human impacts are excluded to consider only the impacts of natural factors on the land cover distribution in this study. However, the land cover distribution could be altered strongly by human activities such as groundwater depletion, deforestation, and grazing. A small portion of area affected by human activities may strongly impact the surrounding land cover distribution (Figure S2 in Supporting Information S1). For this reason, the proportions of built areas and cropland should be constrained to small values.
 - For SPs, (a) the proportion of flooded vegetation exceeds 0 or the climate type is not arid/semiarid. Because these landscapes often appear in terminal lake basins where the climate is extremely hot and dry, the growth of aquatic plants is largely constrained due to water scarcity and saline conditions. (b) An ocean pixel is detected near or in the unit catchment. This rule is used to avoid confusion with another SP type that is distributed in coastal regions and affected mainly by seawater with or without downhill waterflow, such as SPs in tidal salt marshes (Pethick, 1974).
- 7) For the remaining hillslope-dominated landscapes, the elevation range over which hillslope impacts are detected, that is, the relative height of the band in which the final transition occurs, is summarized. To avoid the false detection of landscapes where the vertical land cover distribution is prone to climate impacts, the threshold defining the elevation range of hillslope impacts was determined heuristically to be 100 m (Text S2 in Supporting Information S1). Landscapes in which the elevation range of hillslope impacts exceeds this threshold are excluded.

To illustrate the procedure outlined above, we provide an example of GF detection in Figure 3. The local topography of the unit catchment is shown in Figure 3a. Based on the topography, the catchment-based strategy is used to discretize the catchment into 10 height bands (Figure 3b). The discretized height bands are applied to the high-resolution land cover map (Figure 3c) and the dominant land cover type (Figure 3d) is determined according to the summarized proportion of each land cover type in each band (Figure 3e). The dominant land cover type changes from trees in the first band to scrub/shrubs in the second band, matching the assumed GF transition path (Path I in Table 2) with relatively high proportions of 66% and 59%, respectively. Figure 3e illustrates the elevation range where hillslope impacts were detected, which is near 50 m and below the set 100-m elevation threshold. Using these data in combination with the satellite image (Figure 3f), no built area or cropland is detected nearby, suggesting the development of this landscape with little anthropogenic interference. Overall, these results exemplify the successful detection of a GF that developed mainly under the impact of hillslope water dynamics. Furthermore, the land cover in each band is uniformly represented by the dominant type to generate an aggregated land cover map (Figure 3d). Subsequently, as described in Section 5.1, the accuracy of dominant land cover type representation of catchment-based strategy is determined and compared with that of a simple grid-downscaling method.

3.3. Validation of Detected Landscapes

To validate the landscapes detected as described in Section 3.2, we examine the detection results generated with different PTVs (20%, 30%, 40%, 50%, and 60%) for each transition path listed in Table 2.

In general, fewer landscapes will be detected with higher threshold values; underestimation may occur if the PTV is set too high. To avoid this issue, we compared PTV categories to determine the appropriate PTV for each landscape type based on the point at which the number of detected landscapes reaches peaks and shows little further difference. To improve robustness, the highest PTV among the appropriate values is selected as the optimal threshold and employed to derive the global distribution of the corresponding landscape type.

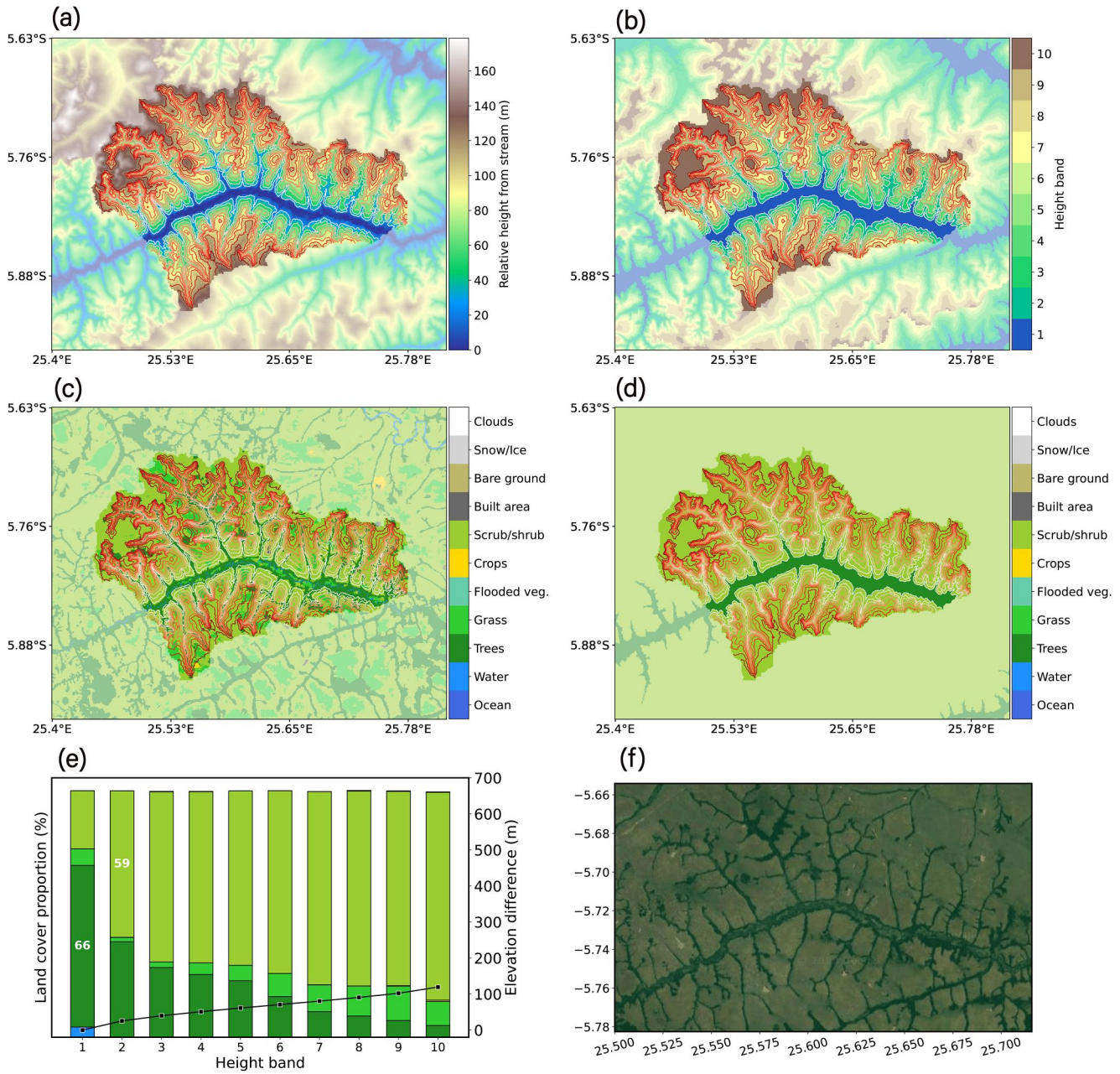


Figure 3. Example of GF detection in Kinda-Mwampu, Congo. (a) Relative height from the mainstream, (b) height bands aggregated through the catchment-based strategy, (c) land cover map, and (d) land cover map aggregated through the application of the catchment-based strategy near the location of the detected landscape. In (a)–(d), the target catchment is highlighted in a brighter color than the surrounding area. In (a) and (c), the boundaries of height bands in the landscape are represented as contours, with redder contours enclosing height bands at higher elevations. (e) Bar plot showing the proportions of land cover types in each height band. Bars with value tags represent the height bands involved in step 3 of the detection procedure, and the values indicate the proportions of dominant land cover types in the bands. The line plot shows the median difference in elevation for each height band relative to the lowest band. (f) Static Google Earth map of the same area.

On the other hand, due to inherent deficiencies in the detection method or baseline data, falsely detected landscapes may be included in the results, leading to overestimation for certain landscape types. To evaluate the risk of overestimation, we visually examine the detected landscapes for each PTV category, identifying false detections and then calculating the detection accuracy (a_{PTV}):

$$a_{PTV} = \frac{m_{PTV}}{n_{PTV}}, \quad (1)$$

where the PTV is 20%, 30%, 40%, 50%, or 60%; m_{PTV} denotes the number of landscapes confirmed to be correct detections by visual examination; and n_{PTV} denotes the number of landscapes selected for visual examination. As the visual examination of all landscapes is difficult when the detection number is large, we randomly select 10% of the detected landscapes for each landscape category as n . Specifically, we examine each selected landscape with reference to the corresponding land cover distribution and satellite image. When the spatial information provided by the reference maps is unclear, we additionally check the location at a smaller scale using Google Earth to confirm whether the landscape has been shaped by hillslope water dynamics. Generally, false detections are identified in the following cases:

- 1) Despite the effort to exclude human impacts during detection, landscapes affected by human factors may be falsely detected. By visual examination, they are identified from the satellite image if the land cover tiles in the area appear as regular mosaic. For example, regularly trimmed woodland is falsely detected as GF in Figure S3 in Supporting Information S1; the land cover distribution pattern has resulted mainly from human activity, rather than hillslope water dynamics.
- 2) The misclassification of land cover type in the Sentinel-2 LULC product may lead to false detection. By visual examination, this type of false detection is identified if any regular boundary line between land cover tiles appears merely in the land cover map but not in the corresponding satellite image in the area. Figure S4 in Supporting Information S1 shows an example of a falsely detected landscape, with an abrupt change of land cover from trees to scrub/shrubs visible in its northern part. The scrub/shrubs present in the highest band have been mistakenly detected as the dominant land cover type due to a classification error.
- 3) Local factors such as soil type, wind, wildfire, aspect, and microclimate driven by microtopography may mediate the land cover distribution in the landscape (Aas et al., 2019); in some cases, the detection method may lead to the false detection of these landscapes as shaped by hillslope water dynamics (e.g., Figure S5 in Supporting Information S1). We identify this type of false detection by visually checking if any vegetated tile is distributed perpendicular to the contours and no stream or pond appears amid the tile.

Generally, the occurrence of these issues is independent of the PTV setting. To robustly evaluate the extent of overestimation, we calculate the mean detection accuracy (\bar{a}) among the five PTV categories:

$$\bar{a} = \frac{a_{20\%} + a_{30\%} + a_{40\%} + a_{50\%} + a_{60\%}}{5}. \quad (2)$$

4. Results

4.1. Global Distribution of Hillslope-Dominated Landscapes

Figure 4 illustrates the global distribution of hillslope-dominated landscapes, derived through the synthesis of the maps for each detected hillslope landscape type (Figures 6a–6e). SP stands out as the most abundant landscape type (3,383 detections worldwide). Overall, the distribution map shows some geographical patterns: SPs occur mainly near 30°N and 30°S, especially in the Northern Hemisphere, and cover a wide range of dry regions including the Sahara Desert and Arabian Peninsula. GFs are located mainly in equatorial regions with semiarid climate conditions, such as Amazonia in South America and the Congo Basin in Central Africa, generally near the border between tropical and dry regions. Some GFs are also detected in subarctic regions, such as Eastern Siberia. The WL and RB distributions overlap with some documented wetland types, such as peatlands and swamps. Unlike RBs, which occur primarily in boreal regions (south of Hudson Bay in Canada and Tomsk Oblast in Russia), WLs cover large areas in boreal (Alaska and Canada in North America, Nordic countries and Russia in Eurasia) and equatorial (Amazonia in South America and the Congo Basin in Central Africa) regions.

In Figure 5, we present zoomed-in views and the properties of example landscapes selected from Figure 4. The SP detected on the land cover map is clearly visible in the satellite image as an expanse of salt evaporites in the northeastern part of the domain (Figure 5a). In an example of DR, a narrow corridor of forest is observed along a winding stream (Figure 5b). Compared to the GF example in Figure 3 that shows an identical transition path to DR landscape in this case (i.e., from trees to grass), virtually identical vegetation patterns are revealed on the land cover maps. However, on the upper hillslope, where the land cover is dominated by scrub/shrubs, the satellite image clearly shows sparser vegetation in the DR than in the GF landscape. This difference suggests that the differentiation of DR and GF landscapes based solely on land cover maps is impossible without the consideration

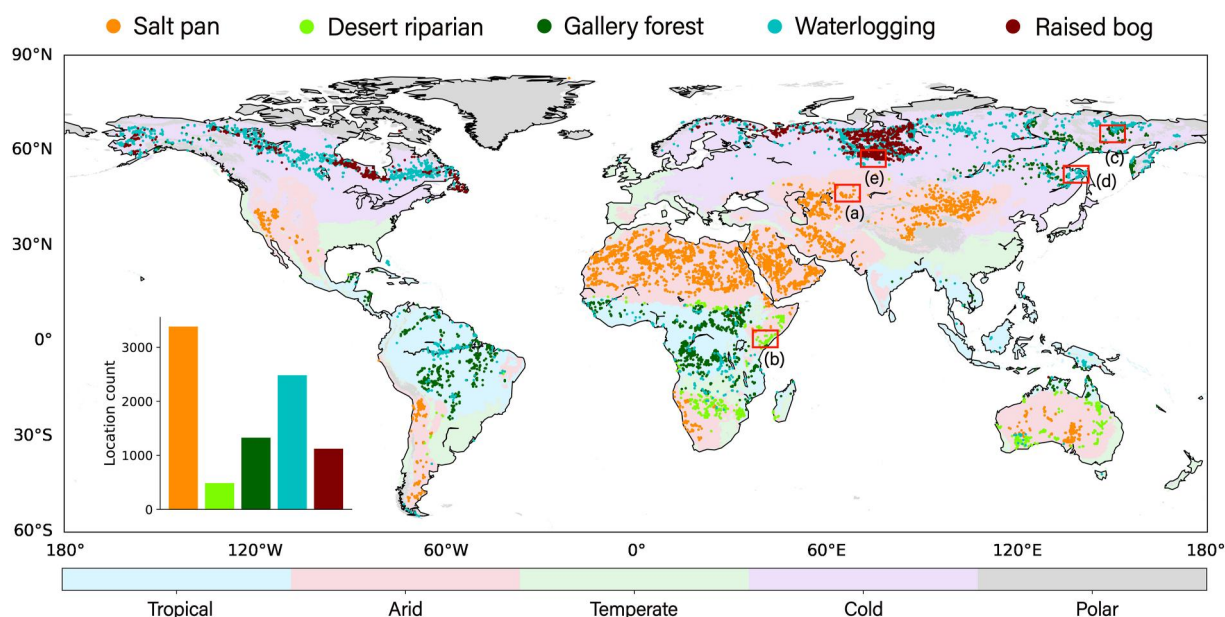


Figure 4. Global distribution of five hillslope-dominated landscape types (derived using the optimal PTV, determined as described in Section 4.2) and global climate classification map (Beck et al., 2018). Locations with overlapping RB and WL are represented by RB. The inset bar plot shows the abundance of each landscape type. Red boxes indicate the locations of the landscape examples presented in Figure 5.

of additional conditions (e.g., wetness or temperature). In addition to the GF example shown in Figure 3, a GF example corresponding to transition Path II, in which the lowest band is represented by water (a stream), is shown in Figure 5c. An example of WL landscape corresponding to transition Path II is shown in Figure 5d, with waterlogging at its center and a change in the dominant land cover type from water to scrub/shrubs and then to trees from low to high bands. For the RB example shown in Figure 5e, the brown area of the satellite image represents waterlogged peatland on lifted mounds. Note that in some cases, WL landscapes are detected in lower height bands while RBs are detected in both lower and higher height bands of the unit catchment, constituting simultaneous detection (Figure S7 in Supporting Information S1). This phenomenon explains the few overlapping areas in the WL and RB distributions in Figure 4.

According to the lines plots in the middle panels of Figure 5, despite differences in topography among landscapes, land cover transitions with relatively flat topography are observed across lower height bands in areas where vegetation patterns are affected by hillslope water dynamics, for example, the lowest three bands in the WL landscape (Figure 5d). Notably, a hillslope impact is observed for the topographically flat RB, in which the elevation difference across all height bands is less than 20 m. This finding suggests that the force of gravity causes hillslope water dynamics to perturb or control the spatial pattern of vegetation in catchments with overall complex topography but relatively flat terrain in the lower hillslope area, in addition to flat catchments. It illustrates the widespread occurrence of hillslope impacts across numerous terrestrial regions.

In some unit catchments, hillslope and climate impacts are observed simultaneously. For some unit catchments detected as GF, the dominant land cover type first changes from trees to shrubs, and then shifts back from shrubs to trees in the highest band (Figure S6a in Supporting Information S1). The same phenomenon is observed in other landscape types, such as WL landscapes (Figure S6b in Supporting Information S1), where the dominant land cover type first changes from water and shrubs to trees, and then shifts back from trees to shrubs in the highest band. This pattern is probably due to the impacts of climatic factors, as the elevation difference between the highest and lowest bands of the unit catchment far exceeds 100 m. Thus, the land cover distribution in the same catchment is likely affected simultaneously by hillslope and climate impacts when the elevation difference is very large. To focus on the analysis of hillslope impacts, we labeled such unit catchments as hillslope-dominated landscapes and included them in the distribution results for hillslope-dominated landscapes depicted in Figure 4.

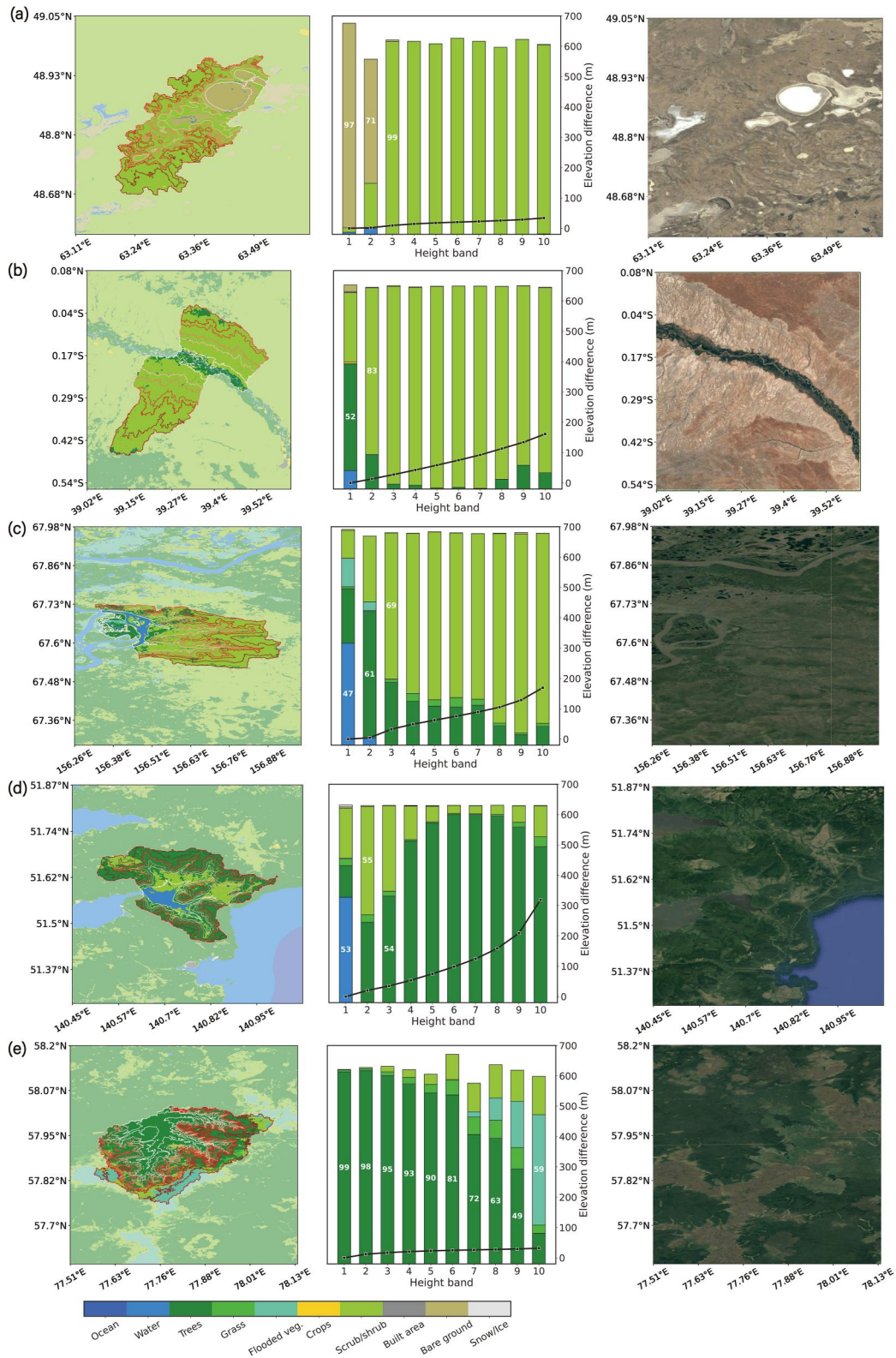


Figure 5.

4.2. Validation of the Detected Landscapes

Figure 6 shows the validation results for the detected landscapes. The number of detections peaks for SP and DR landscapes when the PTV is set to 20%, 30% or 40% (Figures 6a and 6b), and for GF, WL, and RB landscapes when the PTV is set to 20% or 30% (Figures 6c–6e). Thus, the PTV can be set higher (40%) for the detection of SP and DR landscapes than for the detection of GF, WL, and RB landscapes, indicating a more distinct pattern of transition in dominant land cover type along the hillslope for the former. Despite minor differences in detection numbers, we considered the highest PTV among all appropriate PTVs to be optimal to ensure the robustness of the results; that is, the PTV is set to 40%, 40%/40%, 30%/30%, 30%/30%, and 30%/30%/30%/30% to derive the global distributions of SP (Path I), DR (Path I/II), GF (Path I/II), WL (Path I/II) and RB (Path I/II/III/IV) landscapes, respectively (Figures 4, 6 and 7, and Figure S11 in Supporting Information S1).

The false detection of landscapes due to human factors, classification errors in the baseline data, and other factors can lead to the overestimation of the distribution of a landscape type. According to Figure 6, mean detection accuracies for all landscape types approximate or exceed 90%, indicating a low likelihood of overestimation. An exception occurs on Path I for DR and GF landscapes, for which the mean detection accuracy is near 85%, indicating a slightly greater possibility of false detection (mainly due to human impacts; Tables S1–S5 in Supporting Information S1) than for other landscape types. In addition, on transition Path II for GFs, greater detection accuracy is observed when the PTV is set to 50% or 60%, but this value is likely to be invalid due to uncertainty in the selected samples. Based on comparison with the landscape detection results obtained with PTVs of 20%, 30% and 40%, PTVs of 50% and 60% were not used for the construction of the distribution map due to evident underestimation.

Overall, the validation results suggest that limited overestimation occurs in landscape detection when the appropriate threshold values are applied to the proportion of dominant land cover type.

5. Discussion

5.1. Comparison of the Spatial Distribution of Hillslope-Dominated Landscapes With Previous Research Findings

The landscape map derived in this study largely agrees with distribution information provided in the relevant literature. The derived distribution of SPs shows strong spatial consistency with well-known regions of SP presence around the world (Safaei & Wang, 2020; Schulz et al., 2015), with a small fraction of mismatches in regions such as the west side of the Caspian Sea. The GF results correspond with previously reported GF distribution information, such as that for the Pantanal and Amazonia regions in central South America (Felfili, 1995; Silva et al., 2008) and West Cameroon in Africa (Momo et al., 2018). The distribution patterns derived for WL and RB landscapes are consistent with the Global Lakes and Wetlands Database (Lehner & Döll, 2004), and they overlap with the global peatland distribution map to differing extents (Kirpotin et al., 2021; Xu et al., 2018).

In addition to showing extensive overlap with documented landscape locations, the newly derived landscape map shows some landscapes that have not, to our knowledge, been previously reported. For example, we identified previously undocumented GFs in eastern Siberia (Figure 5). Although plant growth is limited by energy (e.g., radiance and temperature) across the high-latitude regions of Eurasia (Li et al., 2021), a massive amount of dry air accumulates in the east and far east of Siberia, creating seasonal water-limited conditions (Beck et al., 2018). This regional water limitation may enhance the impact of hillslope water dynamics on vegetation patterns, leading to GF development in this region. Interestingly, in the Horn of Africa, where the climate is semiarid, a cluster of previously unreported DR landscapes was detected (Figure 5). According to the global pattern of groundwater table depths (Fan et al., 2013), the water table is relatively shallow in this region relative to that in the surrounding

Figure 5. Examples of detected (a) SP (Southern Kostanay region, Kazakhstan), (b) DR (Horn of Africa), (c) GF (northeastern Russia), (d) WL (Lake Ozero Maloye Kizi, Russia) and (e) RB (eastern Tomsk Oblast, Russia) landscapes. On the land cover maps (left), the detected landscapes are highlighted with a brighter color than the surrounding area. The boundaries of height bands in the landscapes are represented as contours, with redder contours enclosing height bands at higher elevations. The bar plots in the middle show the proportions of land cover types in each height band. Bars with value tags represent the height bands used in the identification procedure, and values indicate the proportions of the dominant land cover types in the corresponding height bands. The plotted lines show the median difference in elevation between each height band and the lowest band. Static Google Earth maps (right) show satellite images of the same areas as the land cover maps.

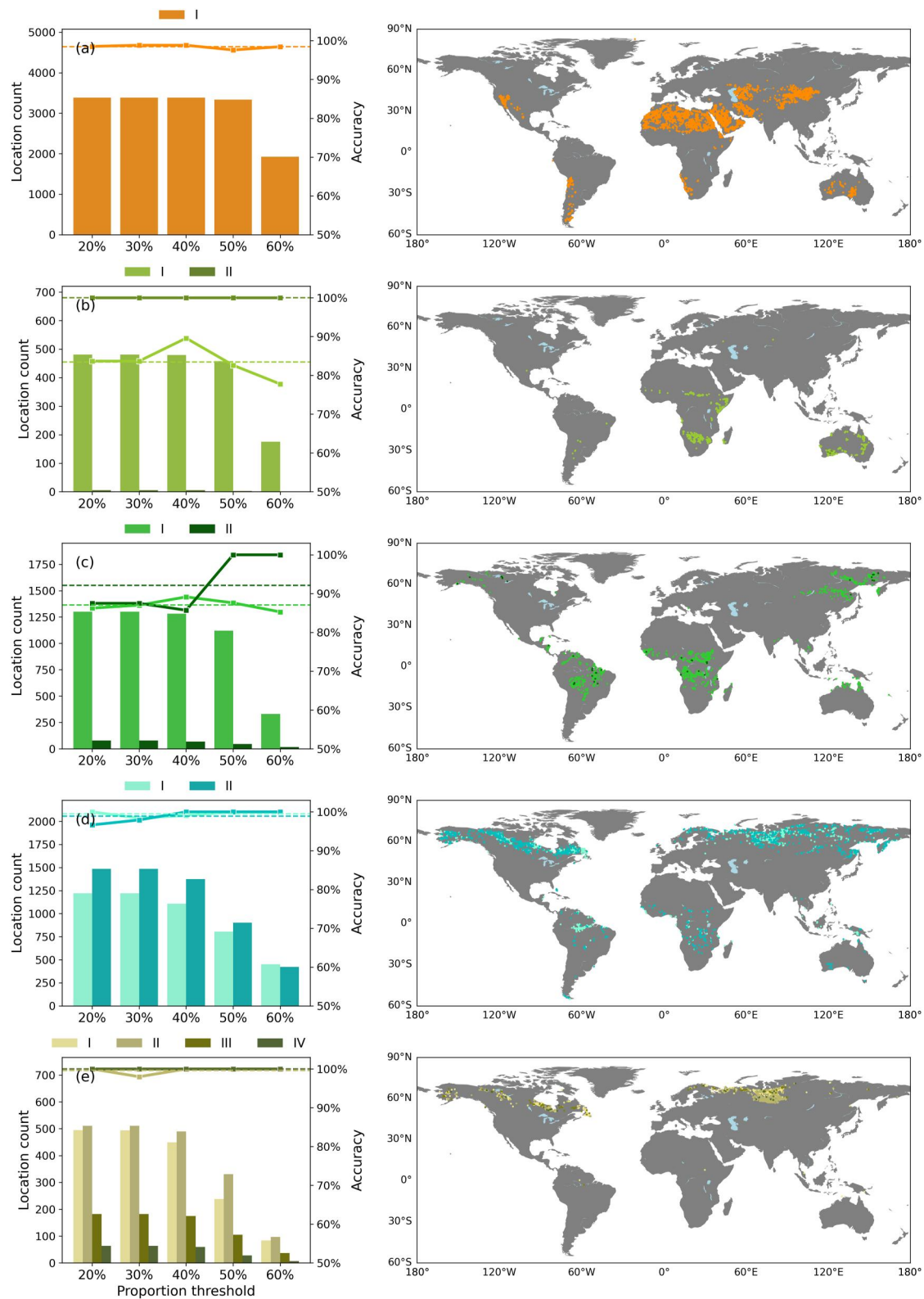


Figure 6. Validation of the global distributions of (a) SP, (b) DR, (c) GF, (d) WL, and (e) RB landscapes associated with five PTV categories. In the left panels, bar plots show the number of landscapes detected for each category. Solid and dashed lines denote the detection accuracy of each PTV category and the mean detection accuracy among PTV categories, respectively. The right panels show the distribution of detected landscapes generated using the optimal PTV. Detailed information about accuracy evaluation is provided in Tables S1–S5 in Supporting Information S1.

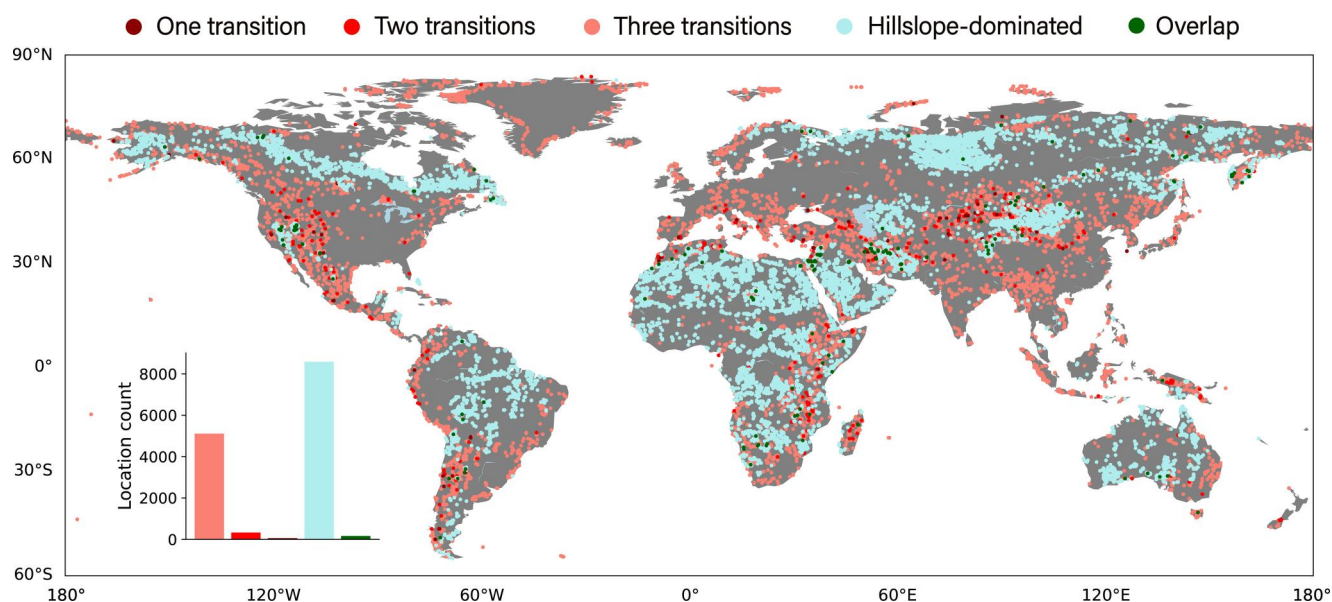


Figure 7. Global distributions of hillslope-dominated landscapes (blue) and climate-dominated landscapes with transition patterns of one (light red), two (red), and three (dark red) changes in the dominant land cover (climate) type. Areas of overlap between climate- and hillslope-dominated landscape types are represented with green dots. The inset bar plot indicates the number of each landscape type.

area. This finding reflects the convergence of groundwater in low valleys due to hillslope water dynamics, which may contribute to DR landscape development.

5.2. Comparison With the Distribution of Climate-Dominated Landscapes

The strategy proposed here for the detection of hillslope-dominated landscapes can also be applied to the search for climate-dominated landscapes (Figure 1a). Unlike hillslope-dominated landscapes, where vertical land cover transitions occur within the same climate zone, vertical land cover transitions in climate-dominated landscapes occur with climate zone transitions. In addition to the map of hillslope-dominated landscape distribution presented in Figure 4, the global distribution of climate-dominated landscapes was derived (Figure 7; the procedure is described in Text S3 in Supporting Information S1). High consistency is apparent between the distributions of climate-dominated landscapes and mountainous areas globally, such as the Sierra Nevada Mountains in the western US and the Andes Mountains of South America (von Humboldt, 1807), and especially for landscapes with multiple transitions in the dominant land cover (climate) type (red and dark red dots). Figure 7 also shows the locations where climate- and hillslope-dominated landscapes overlap (examples shown in Figure S8 in Supporting Information S1), most of which are distributed near the boundary between the two landscape types.

About 5,500 climate-dominated landscapes were detected worldwide, indicating that the global coverage of these landscapes is smaller than that of hillslope-dominated landscapes (~8,500). This result suggests that hillslope water dynamics have had more extensive impacts than climatic factors on sub-grid land cover heterogeneity, and provides further evidence of the importance of investigating these impacts. When deriving the global distributions of the five hillslope-dominated landscape types shown in Figure 4, the application of the strict proportion threshold (1%) for anthropogenic land cover types, that is, built area and cropland, leads to the masking out of a large number (2,240) of catchments. Nevertheless, in catchments where anthropogenic and natural land cover types coexist, hillslope impacts may perturb the vegetation pattern to some extent. For this reason, the impacts of hillslope water dynamics on global land cover heterogeneity may be broader than observed for the mapped hillslope-dominated landscapes (Figure 4).

Overall, the broad coverage of hillslope- and climate-dominated landscapes highlights the importance of resolving sub-grid heterogeneity in LSMs for the more accurate simulation of land surface processes at small scales.

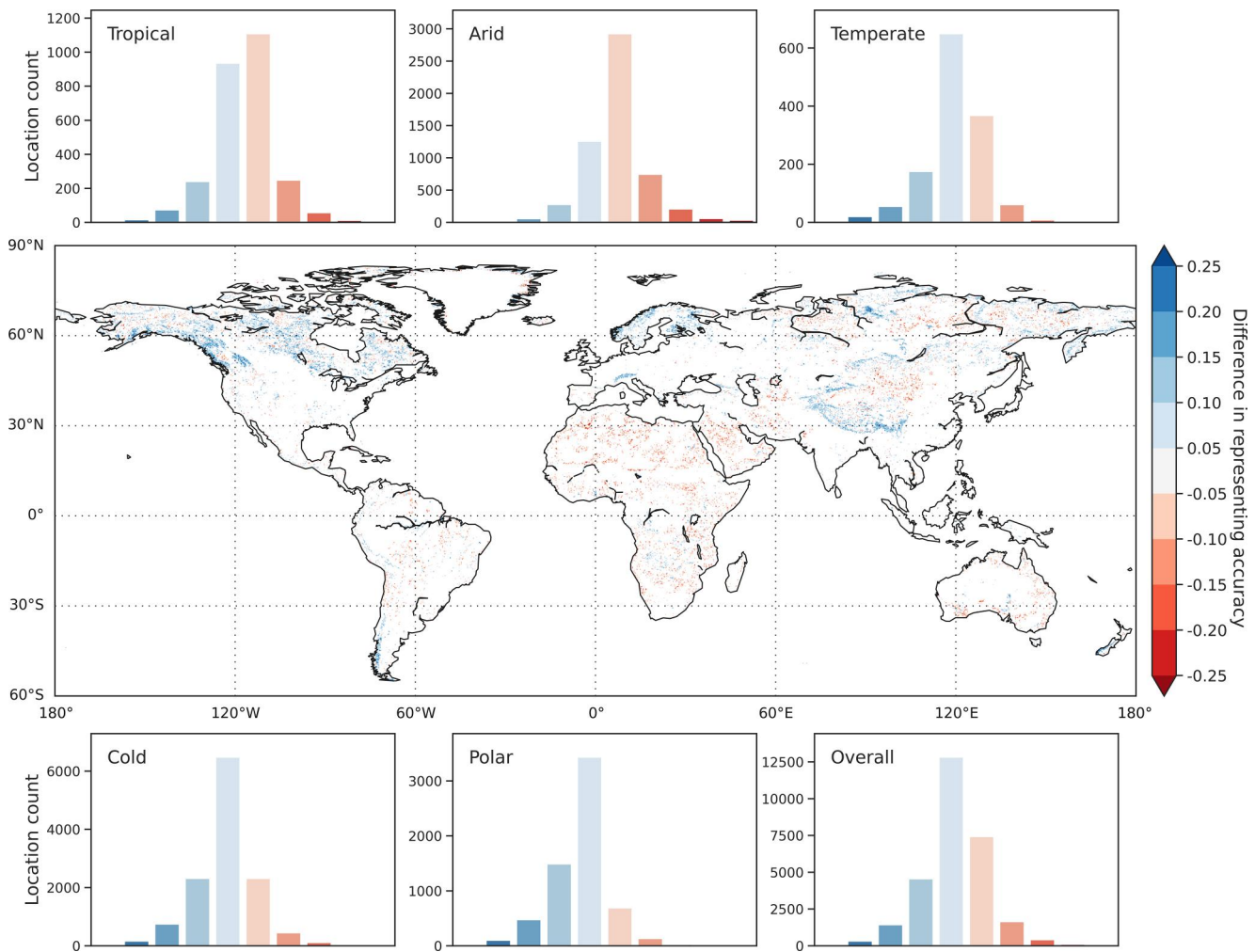


Figure 8. Difference in the accuracy of land cover heterogeneity (φ_{dif}) representation between the catchment-based and grid-downscaling methods. Positive (φ_{dif}) values denote more accurate representation with the catchment-based strategy than with the grid-downscaling method, and negative (φ_{dif}) values indicate greater accuracy with the grid-downscaling method than with the catchment-based strategy. The bar plots show the numbers of locations corresponding to various levels of difference in representation accuracy for tropical, arid, temperate, cold, and polar climate types and globally. The categories represented with bars of different colors match those on the global map.

5.3. Representation of Land Cover Heterogeneity in the LSM

To investigate the merit of accurately resolving explicit land cover heterogeneity, the catchment-based strategy is compared with the downscaling of a rectangular grid from larger to smaller units. Specifically, we compare the ability of 10 height bands and 3×3 rectangular grid units to approximate the explicit land cover distribution, as described in Supplementary Text S4 in Supporting Information S1. The explicit land cover heterogeneity is concisely resolved by assigning the dominant land cover type to the entire calculation unit (height band or grid cell, respectively). This use of the dominant land cover type to represent land cover heterogeneity inevitably leads to inaccurate representation. Thus, we determined the accuracy of representations obtained using the two strategies by averaging the accuracies calculated in each calculation unit (height band or grid cell, respectively), then we calculate the difference (φ_{dif}) between the two averaged values. Despite minor differences (between -0.05 and 0.05) for most locations, the φ_{dif} values reveal geographic patterns (Figure 8).

The catchment-based strategy provides significantly more accurate representations of land cover heterogeneity in flat regions with humid conditions (e.g., northern Siberia and Canada, as well as river mainstems and major tributaries in Amazonia, where WL landscapes are widespread) and regions with high topographic relief (e.g., the Tibetan Plateau and Alps). In topographically flat regions where the climate is homogeneously wet, the

catchment-based strategy effectively captures vertical land cover gradients shaped by hillslope water dynamics. In regions with high topographic relief where the climate is distinctly heterogeneous, the catchment-based strategy also generates more accurate representations, indicating that vegetation patterns induced by climate impacts align strongly with the topographic gradient.

On the other hand, the proposed strategy generates less accurate representations of land cover heterogeneity in flat regions with arid climates (e.g., the Sahara and Arabian Peninsula). Separately, the representation by the catchment-based strategy is favorably accurate (Figure S9 in Supporting Information S1), justifying the extensive detection of SPs in the corresponding regions (Figure 4). Despite the better infiltration conditions in flat terrain than in high-relief terrain due to longer residence of surface water (Han et al., 2020; Huang et al., 2018), the unpronounced hillslope water dynamics impedes water convergence in lowland valleys and may have resulted in reduced accuracy. In addition, an extremely dry climate leads to substantial evaporation and thus insufficient moisture for plant uptake in the soil root zone. These two factors may collectively attenuate the impact of hillslope water dynamics on local vegetation patterns, explaining the lesser accuracy of representations obtained using the catchment-based strategy.

Overall, with the masking out of locations with trivial differences in representation accuracy, the ratios of locations labeled in blue (more accurate representation with the catchment-based strategy) and red (less accurate representation with the catchment-based strategy) to total locations are 67% and 33%, respectively. These results indicate that the proposed strategy has the advantage of resolving explicit land cover heterogeneity shaped by both climate and hillslope impacts over the simple downscaling of an equivalent size of rectangular grid to 9 sub-grids. With that being said, we note that the current comparison method does not account for the source of the difference, which may be the result of the different shapes of unit catchment and rectangular grid or the discretization of them into different shapes of unit (i.e., height bands vs. rectangular sub-grids), or both. Further comparison between the grid-based height bands and grid-based rectangular sub-grids is needed if the source of the difference were to be distinguished.

5.4. Limitations of the Catchment-Based Strategy

Some landscapes reported in previous studies are absent from Figure 4. For example, as a typical desert vegetation type in the southwestern US, DR landscapes have been frequently studied at the regional scale (Hultine et al., 2015; Nguyen et al., 2015). The impact of waterlogged conditions on plant growth in temperate regions across North and South America, Europe, and South and East Asia has been discussed intensely (Schulz et al., 2015; Zúñiga-Feest et al., 2017). Nevertheless, only a fraction of WL landscapes was detected in Scotland, UK; Tasmania, Australia; and New Zealand (Figure 4). Missed detection of the five landscape types may be attributed to the following reasons:

- 1) There exist various sizes of landscapes, whose spatial coverage may range from a few hundred meters to several kilometers. Any pre-defined unit catchment size might be too coarse or too fine to detect landscapes that are visible on satellite imagery. On the one hand, when the unit catchment is relatively large in size and discretized into coarse height bands, the explicit land cover distribution may be represented inaccurately by the dominant land cover type (Figure S10 in Supporting Information S1). This issue arises because the catchment-based strategy treats the lower height band as the “mainstem” and secondary tributaries as part of the hillslope. Although the satellite imagery shows that trees also line along secondary tributaries (Figure 3f), these trees are not resolved accurately using the given height bands (Figure 3d). Hence, land cover heterogeneity remains partially resolved, which could possibly result in non-detection of potential landscapes. With the development of a finely discretized boundary map of unit catchments and treatment of tributaries as “mainstem” areas, further improvement of the representation accuracy detection of additional landscapes can be expected. On the other hand, when the size of unit catchment is relatively small, it might capture only a fragmentary part of the landscape shown in the satellite imagery and fail to discern the transition of dominant land covers along hillslope. Likewise, it could lead to non-detection. Aside from hillslope water dynamics, other factors such as wind, wildfires, and the hillslope aspect affect local vegetation patterns in various manners (Fan et al., 2019; Gerlach, 1993; Smith & Finch, 2018). To represent this heterogeneity and thereby improve the proposed strategy, multiple tiles in each height band could be used to represent different hydrological response units (Chaney et al., 2018).

- 2) Landscape detection with the current catchment-based strategy begins from the lowest band, focusing on the identification of landscapes on the lower part of the hillslope. The detection procedure terminates when a change in climate type occurs. However, the climate in alpine regions could exhibit significant vertical heterogeneity within single unit catchments (Beck et al., 2018). Water dynamics may have a greater impact on the middle or upper part of the hillslope when they control vegetation patterns in those areas (von Humboldt, 1807; Zou et al., 2023).
- 3) The exclusion of anthropogenic factors can lead to incomplete detection results. In the southwestern US and many other places, built areas and croplands are often located near riparian areas due to their proximity to stream water. Anthropogenic land coverage is large in temperate regions due to the favorable climate conditions. Human influence explains the missed detection of a large number of landscapes in Figure 4. This finding may reflect the substantial underestimation of hillslope impacts, as hillslope water dynamics also have great impacts on the natural distribution of land cover types in unit catchments where human impacts are less significant.
- 4) The limitations of baseline land cover data also hinder accurate detection. The distribution of hillslope-dominated landscapes was derived from a composite intra-annual land cover product (Table 1). Landscapes influenced by seasonal changes in land cover might be neglected in that dataset. For example, in temperate regions where precipitation has a strong seasonal pattern, seasonally flooded WL landscapes are observed widely during the rainy season. These conditions place a significant constraint on local vegetation, but are not represented in the derived map (Fan et al., 2017; Schulz et al., 2015). Aside from discrepancies between land cover types, different sub-categories of the same land cover type may differ in their adaptation to extreme water conditions. However, different sub-categories of land cover in the LULC dataset have been merged into general types (e.g., broadleaf, needle-leaf, and alpine trees are all categorized as “tree”). The lack of representation of such sub-categories affected the detection results as well.

In light of the above caveats, we emphasize that we did not intend to create a map that perfectly incorporates all landscape locations in this study. Rather, this study provides an overview of landscapes that are influenced by hillslope water dynamics and an unprecedented global inventory of locations with such landscapes (Figure 4). The results underline the crucial role of hillslope impacts in shaping various landscape types that hold hydrological and ecological significance.

6. Conclusion

In this study, a globally applicable catchment-based strategy is proposed to concisely resolve explicit land cover heterogeneity using discretized height bands along hillslopes. Our results show that:

- 1) Using the catchment-based strategy, we present an unprecedented global inventory of landscapes in which the vegetation pattern is shaped by hillslope water dynamics. The validated detection results for hillslope-dominated landscapes show high overall accuracy.
- 2) The detected hillslope-dominated landscapes have wide global coverage. Compared with climate factors, hillslope water dynamics affect vegetation patterns more extensively around the world.
- 3) Some landscapes, for example, GFs in northeastern Russia and DR in the Horn of Africa, are newly revealed in this study. These findings demonstrate the strong impact of hillslope water dynamics on vegetation patterns in dry boreal and semiarid regions.
- 4) The proposed strategy more accurately resolves land cover heterogeneity than does the simple downscaling of a rectangular grid from larger to smaller units. In 67% of terrestrial areas with a distinct difference in representation accuracy, the proposed strategy provides more accurate representation of explicit land surface heterogeneity.

Some hillslope-dominated landscapes, such as DR and GFs, occur near the boundary between climate classification zones, and thus are susceptible to climate change (Figure S11 in Supporting Information S1). Climate change in the coming decades could profoundly affect the status of those landscapes (Beck et al., 2018; Hagedorn et al., 2019). To investigate their spatiotemporal variation patterns from the past to the future, comprehensive elucidation of the underlying mechanism and proper inclusion in LSMs are essential.

Classic LSMs provide lower boundary conditions to the atmosphere, and thus address vertical fluxes at a coarse scale and are incapable of tracing water at and near the land surface. The wide global coverage of hillslope-dominated landscapes indicates the extensive water constraint on vegetation pattern, implying the necessity of

simulating lateral flow in LSMs to resolve the sub-grid heterogeneity caused by hillslope water dynamics. Applying the proposed catchment-based strategy in existing LSMs could be one approach to address the issue. However, note that the current strategy might not effectively solve the land surface heterogeneity caused by other factors such as human activity (e.g., agriculture and urban land). For that purpose, one possible solution is to implement the conventional tile scheme in addition to the catchment-based strategy, which discretizes height band to finer tiles to capture the land surface heterogeneity at smaller scale than height band (Chaney et al., 2018).

Overall, we present the extensive global distribution of landscapes shaped by hillslope water dynamics, which underscores the importance of the explicit resolution of sub-grid heterogeneity in land surface modeling.

Conflict of Interest

The authors declare no conflicts of interest relevant to this study.

Data Availability Statement

The MERIT DEM topography data is accessible at http://hydro.iis.u-tokyo.ac.jp/~yamadai/MERIT_DEM/. The MERIT Hydro hydrography data is accessible at http://hydro.iis.u-tokyo.ac.jp/~yamadai/MERIT_Hydro/. The LULC Sentinel-2 land cover dataset is obtained from <https://livingatlas.arcgis.com/landcover/>. The Koppen-Geiger climate map is available at www.gloh2o.org/koppen/. All links are valid as of 23 March 2024.

Acknowledgments

We express appreciation for the valuable comments and suggestions on developing mechanism of hillslope-impact landscape by Professor Ying Fan. In addition, we are thankful to three anonymous reviewers for providing comments that improved the manuscript. This research was partially supported by JSPS KAKENHI (21H05002) and by MEXT program for the advanced studies of climate change projection (SENTAN: JPMXD0722680395). S Li acknowledges funding from a PhD scholarship from Ministry of Education, Culture, Science, Sports and Technology of Japan (MEXT) and the support from the China Scholarship Council.

References

- Aas, K. S., Martin, L., Nitzbon, J., Langer, M., Boike, J., Lee, H., et al. (2019). Thaw processes in ice-rich permafrost landscapes represented with laterally coupled tiles in a land surface model. *The Cryosphere*, 13(2), 591–609. <https://doi.org/10.5194/tc-13-591-2019>
- Ajami, H., Khan, U., Tuteja, N. K., & Sharma, A. (2016). Development of a computationally efficient semi-distributed hydrologic modeling application for soil moisture, lateral flow and runoff simulation. *Environmental Modelling and Software*, 85, 319–331. <https://doi.org/10.1016/j.envsoft.2016.09.002>
- Bacmeister, J. T., Reed, K. A., Hannay, C., Lawrence, P., Bates, S., Truesdale, J. E., et al. (2018). Projected changes in tropical cyclone activity under future warming scenarios using a high-resolution climate model. *Climatic Change*, 146(3), 547–560. <https://doi.org/10.1007/s10584-016-1750-x>
- Beck, H. E., Zimmermann, N. E., McVicar, T. R., Vergopolan, N., Berg, A., & Wood, E. F. (2018). Present and future köppen-geiger climate classification maps at 1-km resolution. *Scientific Data*, 5, 1–12. <https://doi.org/10.1038/sdata.2018.214>
- Burton, C., Betts, R., Cardoso, M., Feldpausch, T. R., Harper, A., Jones, C. D., et al. (2019). Representation of fire, land-use change and vegetation dynamics in the Joint UK Land Environment Simulator vn4. 9 (JULES). *Geoscientific Model Development*, 12(1), 179–193. <https://doi.org/10.5194/gmd-12-179-2019>
- Chaney, N. W., Huijgevoort, M. H. J. V., Shevliakova, E., Malyshev, S., Milly, P. C. D., Gauthier, P. P. G., & Sulman, B. N. (2018). Harnessing big data to rethink land heterogeneity in Earth system models. *Hydrology and Earth System Sciences*, 22(6), 3311–3330. <https://doi.org/10.5194/hess-22-3311-2018>
- Chaney, N. W., Metcalfe, P., & Wood, E. F. (2016). HydroBlocks: A field-scale resolving land surface model for application over continental extents. *Hydrological Processes*, 30(20), 3543–3559. <https://doi.org/10.1002/hyp.10891>
- Clark, M. P., Fan, Y., Lawrence, D. M., Adam, J. C., Bolster, D., Gochis, D. J., et al. (2015). Improving the representation of hydrologic processes in Earth System Models (pp. 5929–5956). <https://doi.org/10.1002/2015WR017096>
- Fan, Y., Clark, M., Lawrence, D. M., Swenson, S., Band, L. E., Brantley, S. L., et al. (2019). Hillslope hydrology in global change research and earth system modeling. *Water Resources Research*, 55(2), 1737–1772. <https://doi.org/10.1029/2018WR023903>
- Fan, Y., Duffy, C. J., & Oliver, D. S. (1997). Density-driven groundwater flow in closed desert basins: Field investigations and numerical experiments. *Journal of Hydrology*, 196(1–4), 139–184. [https://doi.org/10.1016/S0022-1694\(96\)03292-1](https://doi.org/10.1016/S0022-1694(96)03292-1)
- Fan, Y., Li, H., & Miguez-Macho, G. (2013). Global patterns of groundwater table depth. *Science*, 339(6122), 940–943. <https://doi.org/10.1126/science.1229881>
- Fan, Y., Miguez-Macho, G., Jobbágy, E. G., Jackson, R. B., & Otero-Casal, C. (2017). Hydrologic regulation of plant rooting depth. *Proceedings of the National Academy of Sciences of the United States of America*, 114(40), 10572–10577. <https://doi.org/10.1073/pnas.1712381114>
- Felfili, J. M. (1995). Diversity, structure and dynamics of a gallery forest in central Brazil. *Vegetatio*, 117, 1–15. <https://doi.org/10.1007/bf00033255>
- Fisher, R. A., & Koven, C. D. (2020). Perspectives on the future of land surface models and the challenges of representing complex terrestrial systems. *Journal of Advances in Modeling Earth Systems*, 12(4). <https://doi.org/10.1029/2018MS001453>
- Gao, H., Hrachowitz, M., Fenicia, F., Gharari, S., & Savenije, H. H. G. (2014). Testing the realism of a topography-driven model (FLEX-Topo) in the nested catchments of the Upper Heihe, China. *Hydrology and Earth System Sciences*, 18(5), 1895–1915. <https://doi.org/10.5194/hess-18-1895-2014>
- Gao, H., Sabo, J. L., Chen, X., Liu, Z., Yang, Z., Ren, Z., & Liu, M. (2018). Landscape heterogeneity and hydrological processes: A review of landscape-based hydrological models. *Landscape Ecology*, 33(9), 1461–1480. <https://doi.org/10.1007/s10980-018-0690-4>
- Gerlach, J. (1993). Invasive melastomataceae in Seychelles. *Oryx*, 27(1), 22–26. <https://doi.org/10.1017/s0030605300023917>
- Hagedorn, F., Gavazov, K., & Alexander, J. M. (2019). Above- and belowground linkages shape responses of mountain vegetation to climate change. *Science*, 1123(September), 1119–1123. <https://doi.org/10.1126/science.aax4737>
- Han, Z., Chen, X., Huang, Y., Luo, B., Xing, H., & Huang, Y. (2020). Effect of slope gradient on the subsurface water flow velocity of sand layer profile. *Journal of Mountain Science*, 17(3), 641–652. <https://doi.org/10.1007/s11629-019-5644-z>
- Hazenberg, P., Fang, Y., Broxton, P., Gochis, D., Niu, G., Pelletier, J. D., et al. (2015). A hybrid-3D hillslope hydrological model for use in Earth system models. *Water Resources Research*, 51(10), 8218–8239. <https://doi.org/10.1002/2014wr016842>

- Huang, Y., Chen, X., Li, F., Zhang, J., Lei, T., Li, J., et al. (2018). Velocity of water flow along saturated loess slopes under erosion effects. *Journal of Hydrology*, *561*, 304–311. <https://doi.org/10.1016/j.jhydrol.2018.03.070>
- Hultine, K. R., Bean, D. W., Dudley, T. L., & Gehring, C. A. (2015). Species introductions and their cascading impacts on biotic interactions in desert riparian ecosystems. *Integrative and Comparative Biology*, *55*(4), 587–601. <https://doi.org/10.1093/icb/fcv019>
- Karra, K., Kontgis, C., Statman-Weil, Z., Mazzariello, J. C., Mathis, M., & Brumby, S. P. (2021). *Global land use/land cover with Sentinel 2 and deep learning*. In *2021 IEEE International Geoscience and Remote Sensing Symposium IGARSS* (pp. 4704–4707). IEEE.
- Kay, J. E., Deser, C., Phillips, A., Mai, A., Hannay, C., Strand, G., et al. (2015). The Community Earth System Model (CESM) large ensemble project: A community resource for studying climate change in the presence of internal climate variability. *Bulletin of the American Meteorological Society*, *96*(8), 1333–1349. <https://doi.org/10.1175/bams-d-13-00255.1>
- Kirpotin, S. N., Antoshkina, O. A., Berezin, A. E., Elshehawi, S., Feurdean, A., Lapshina, E. D., et al. (2021). Great Vasyugan Mire: How the world's largest peatland helps addressing the world's largest problems. *Ambio*, *50*(11), 2038–2049. <https://doi.org/10.1007/s13280-021-01520-2>
- Lawrence, D. M., Fisher, R. A., Koven, C. D., Oleson, K. W., Swenson, S. C., Bonan, G., et al. (2019). The Community Land Model Version 5: Description of new features, benchmarking, and impact of forcing uncertainty. *Journal of Advances in Modeling Earth Systems*, *11*(12), 4245–4287. <https://doi.org/10.1029/2018MS001583>
- Lehner, B., & Döll, P. (2004). Development and validation of a global database of lakes, reservoirs and wetlands. *Journal of Hydrology*, *296*(1–4), 1–22. <https://doi.org/10.1016/j.jhydrol.2004.03.028>
- Li, S., & Sawada, Y. (2022). Soil moisture-vegetation interaction from near-global in-situ soil moisture measurements. *Environmental Research Letters*, *17*(11), 114028. <https://doi.org/10.1088/1748-9326/ac9c1f>
- Li, W., Migliavacca, M., Forkel, M., Walther, S., Reichstein, M., & Orth, R. (2021). Revisiting global vegetation controls using multi-layer soil moisture. *Geophysical Research Letters*, *48*(11). <https://doi.org/10.1029/2021gl092856>
- MacFarlane, W. W., McGinty, C. M., Laub, B. G., & Gifford, S. J. (2017). High-resolution riparian vegetation mapping to prioritize conservation and restoration in an impaired desert river. *Restoration Ecology*, *25*(3), 333–341. <https://doi.org/10.1111/rec.12425>
- MacKay, P. (2013). *Mojave desert wildflowers: A field guide to wildflowers, trees, and shrubs of the Mojave Desert, including the Mojave National Preserve, Death Valley National Park, and Joshua Tree National Park*. Rowman and Littlefield.
- Momo, M. C., Njouonkou, A. L., Temgoua, L. F., Zangmene, R. D., Taffo, J. B. W., & Ntoupka, M. (2018). Land-use/land-cover change and anthropogenic causes around Koupa Matapit Gallery Forest, West-Cameroon. *Journal of Geography and Geology*, *10*(2), 1–56. <https://doi.org/10.5539/jgg.v10n2p56>
- Naudts, K., Ryder, J., McGrath, M. J., Otto, J., Chen, Y., Valade, A., et al. (2015). A vertically discretised canopy description for ORCHIDEE (SVN r2290) and the modifications to the energy, water and carbon fluxes. *Geoscientific Model Development*, *8*(7), 2035–2065. <https://doi.org/10.5194/gmd-8-2035-2015>
- Newman, A. J., Clark, M. P., Winstral, A., Marks, D., & Seyfried, M. (2014). The use of similarity concepts to represent subgrid variability in land surface models: Case study in a snowmelt-dominated watershed. *Journal of Hydrometeorology*, *15*(5), 1717–1738. <https://doi.org/10.1175/jhm-d-13-038.1>
- Nguyen, U., Glenn, E. P., Nagler, P. L., & Scott, R. L. (2015). Long-term decrease in satellite vegetation indices in response to environmental variables in an iconic desert riparian ecosystem: the Upper San Pedro, Arizona, United States. *Ecology*, *84*(4), 610–625. <https://doi.org/10.1002/eco.1529>
- Pethick, J. S. (1974). The distribution of salt pans on tidal salt marshes. *Journal of Biogeography*, *1*(1), 57–62. <https://doi.org/10.2307/3038068>
- Rodríguez-González, P. M., Stella, J. C., Campelo, F., Ferreira, M. T., & Albuquerque, A. (2010). Subsidy or stress? Tree structure and growth in wetland forests along a hydrological gradient in Southern Europe. *Forest Ecology and Management*, *259*(10), 2015–2025. <https://doi.org/10.1016/j.foreco.2010.02.012>
- Roebroek, C. T. J., Melsen, L. A., Van Dijke, A. J. H., Fan, Y., & Teuling, A. J. (2020). Global distribution of hydrologic controls on forest growth. *Hydrology and Earth System Sciences*, *24*(9), 4625–4639. <https://doi.org/10.5194/hess-24-4625-2020>
- Safae, S., & Wang, J. (2020). Towards global mapping of salt pans and salt playas using Landsat imagery: A case study of western United States towards global mapping of salt pans and salt playas using landsat imagery: A case study of western United States ABSTRACT. *International Journal of Remote Sensing*, *41*(22), 8693–8716. <https://doi.org/10.1080/01431161.2020.1781285>
- Schimper, A. F. W., Andreas, F. W., Fisher, W. R., Groom, P., & Balfour, I. B. (1903). *Plant-geography upon a physiological basis (Rev. and e)*. Clarendon Press. Retrieved from <https://www.biodiversitylibrary.org/item/33808>
- Schulz, S., Horovitz, M., Rausch, R., Michelsen, N., Mallast, U., Köhne, M., et al. (2015). Groundwater evaporation from salt pans: Examples from the eastern Arabian Peninsula. *Journal of Hydrology*, *531*, 792–801. <https://doi.org/10.1016/j.jhydrol.2015.10.048>
- Silva, L. C. R., Sternberg, L., Haridasan, M., Hoffmann, W. A., Miralles-Wilhelm, F., & Franco, A. C. (2008). Expansion of gallery forests into central Brazilian savannas. *Global Change Biology*, *14*(9), 2108–2118. <https://doi.org/10.1111/j.1365-2486.2008.01637.x>
- Smith, D. M., & Finch, D. M. (2018). Impacts of interacting fire, climate, and hydrologic changes on riparian forest ecosystems in the Southwest (pp. 32–46).
- Subin, Z. M., Milly, P. C. D., Sulman, B. N., Malyshev, S., & Shevliakova, E. (2014). Resolving terrestrial ecosystem processes along a subgrid topographic gradient for an earth-system model. *Hydrology and Earth System Sciences Discussions*, *11*(7), 8443–8492.
- Swenson, S. C., Clark, M., Fan, Y., Lawrence, D. M., & Perket, J. (2019). Representing intrahillslope lateral subsurface flow in the community land model. *Journal of Advances in Modeling Earth Systems*, *11*(12), 4044–4065. <https://doi.org/10.1029/2019MS001833>
- Tai, X., Anderegg, W. R. L., Blanken, P. D., Burns, S. P., Christensen, L., & Brooks, P. D. (2020). Hillslope hydrology influences the spatial and temporal patterns of remotely sensed ecosystem productivity. *Water Resources Research*, *56*(11), 0–2. <https://doi.org/10.1029/2020wr027630>
- Takata, K., Emori, S., & Watanabe, T. (2003). Development of the minimal advanced treatments of surface interaction and runoff. *Global and Planetary Change*, *38*(1–2), 209–222. [https://doi.org/10.1016/S0921-8181\(03\)00030-4](https://doi.org/10.1016/S0921-8181(03)00030-4)
- van der Velde, Y., Temme, A. J. A. M., Nijp, J. J., Braakhekke, M. C., van Voorn, G. A. K., Dekker, S. C., et al. (2021). Emerging forest–peatland bistability and resilience of European peatland carbon stores. *Proceedings of the National Academy of Sciences*, *118*(38), e2101742118. <https://doi.org/10.1073/pnas.2101742118>
- von Humboldt, A. (1807). *Essay on the geography of plants (English Translation 2009)*. The University of Chicago Press.
- Wood, E. F., Roundy, J. K., Troy, T. J., Van Beek, L. P. H., Bierkens, M. F. P., Blyth, E., et al. (2011). Hyperresolution global land surface modeling: Meeting a grand challenge for monitoring Earth's terrestrial water. *Water Resources Research*, *47*(5). <https://doi.org/10.1029/2010wr010090>
- Xu, J., Morris, P. J., Liu, J., & Holden, J. (2018). PEATMAP: Refining estimates of global peatland distribution based on a meta-analysis. *Catena*, *160*(September 2017), 134–140. <https://doi.org/10.1016/j.catena.2017.09.010>

- Yamazaki, D., Ikeshima, D., Sosa, J., Bates, P. D., Allen, G. H., & Pavelsky, T. M. (2019). MERIT Hydro: A high-resolution global hydrography map based on latest topography dataset. *Water Resources Research*, 55(6), 5053–5073. <https://doi.org/10.1029/2019WR024873>
- Yamazaki, D., Ikeshima, D., Tawatari, R., Yamaguchi, T., O'Loughlin, F., Neal, J. C., et al. (2017). A high-accuracy map of global terrain elevations. *Geophysical Research Letters*, 44(11), 5844–5853. <https://doi.org/10.1002/2017GL072874>
- Yamazaki, D., Oki, T., & Kanae, S. (2009). Deriving a global river network map and its sub-grid topographic characteristics from a fine-resolution flow direction map. *Hydrology and Earth System Sciences*, 13(11), 2241–2251. <https://doi.org/10.5194/hess-13-2241-2009>
- Zou, L., Tian, F., Liang, T., Eklundh, L., Tong, X., Tagesson, T., et al. (2023). Assessing the upper elevational limits of vegetation growth in global high-mountains. *Remote Sensing of Environment*, 286, 113423. <https://doi.org/10.1016/j.rse.2022.113423>
- Zúñiga-Feest, A., Bustos-Salazar, A., Alves, F., Martinez, V., & Smith-Ramirez, C. (2017). Physiological and morphological responses to permanent and intermittent waterlogging in seedlings of four evergreen trees of temperate swamp forests. *Tree Physiology*, 37(6), 779–789. <https://doi.org/10.1093/treephys/tpx023>

References From the Supporting Information

- Al-Khaier, F. (2003). *Soil salinity detection using satellite remote sensing*. ITC.
- Dwivedi, R. S., Sreenivas, K., & Ramana, K. V. (1999). Inventory of salt-affected soils and waterlogged areas: A remote sensing approach. *International Journal of Remote Sensing*, 20(8), 1589–1599. <https://doi.org/10.1080/014311699212623>
- Fan, Y. (2015). Groundwater in the Earth's critical zone: Relevance to large-scale patterns and processes. *Water Resources Research*, 51(5), 3052–3069. <https://doi.org/10.1002/2015wr017037>
- Fluet-Chouinard, E., Stocker, B. D., Zhang, Z., Malhotra, A., Melton, J. R., Poulter, B., et al. (2023). Extensive global wetland loss over the past three centuries. *Nature*, 614(7947), 281–286. <https://doi.org/10.1038/s41586-022-05572-6>
- Leifeld, J., & Menichetti, L. (2018). The underappreciated potential of peatlands in global climate change mitigation strategies. *Nature Communications*, 9(1), 1071. <https://doi.org/10.1038/s41467-018-03406-6>
- Page, S. E., Rieley, J. O., & Banks, C. J. (2011). Global and regional importance of the tropical peatland carbon pool. *Global Change Biology*, 17(2), 798–818. <https://doi.org/10.1111/j.1365-2486.2010.02279.x>
- Scharlemann, J. P. W., Tanner, E. V. J., Hiederer, R., & Kapos, V. (2014). Global soil carbon: Understanding and managing the largest terrestrial carbon pool. *Carbon Management*, 5(1), 81–91. <https://doi.org/10.4155/cmt.13.77>
- Shrestha, D. P., & Farshad, A. (2009). *Mapping salinity hazard: An integration application of remote sensing and modeling based techniques*. In A. J. Zinck & G. Metternich (Eds.), CRC Press (Taylor and Francis).
- Yu, Z., Beilman, D. W., Frohling, S., MacDonald, G. M., Roulet, N. T., Camill, P., & Charman, D. J. (2011). Peatlands and their role in the global carbon cycle. *Eos, Transactions American Geophysical Union*, 92(12), 97–98. <https://doi.org/10.1029/2011eo120001>
- Yu, Z. C. (2012). Northern peatland carbon stocks and dynamics: A review. *Biogeosciences*, 9(10), 4071–4085. <https://doi.org/10.5194/bg-9-4071-2012>
- Zou, J., Ziegler, A. D., Chen, D., Mcnicol, G., Ciais, P., Jiang, X., et al. (2022). Rewetting global wetlands effectively reduces major greenhouse gas emissions. <https://doi.org/10.1038/s41561-022-00989-0>